Title
Simulating irradiance enhancement dependence on cloud optical depth and solar zenith angle

Authors
Pecenak, Zachary K
Mejia, Felipe A
Kurtz, Ben
et al.

Publication Date
2016-10-01

DOI
10.1016/j.solener.2016.07.045

Peer reviewed

Simulating Irradiance Enhancement Dependence on Cloud Optical Depth and Solar Zenith Angle

Authors: Zachary K. Pecenak, Felipe A. Mejia, Amato Evan, Jan Kleissl

Corresponding author:
Zachary K. Pecenak
zpecenak@ucsd.edu
7709 ludington pl, La Jolla, CA 92037

Keywords: Irradiance Enhancement; Over-irradiance; Monte Carlo RTM;

Abstract

Enhancement of solar irradiance (IE) has been observed in many locations under partly cloudy sky conditions. Despite its notoriety, few studies have attempted to systematically examine the underlying mechanism for the event through simulation. As a result, there is no consensus regarding the causes of IE, nor an understanding of the effects of cloud optical depth and/or solar elevation on the event. Using a 2D Monte Carlo radiative transfer model (RTM), we show that IE through a homogenous square cloud is caused by the superposition of a direct irradiance beam with diffuse light scattered through the bottom and out of the edge of a cloud, through Mie scattering. Using the RTM, we investigated the effect of optical depth up to 500 and solar zenith angles ranging from 0 to 60 degrees on the IE magnitude and spatial extent. For the overhead zenith case the IE magnitude is maximum between optical depths of 20 and 50, with a value of 1.27 times the clear sky value. IE magnitude increases monotonically with increasing solar zenith angle, with the maximum occurring at a higher optical depth. The greatest magnitude overall occurred for a solar zenith angle 60 degrees (our maximum) and optical depth of 100, with a value of 1.7 times the clear sky value. The simulation show that optically thick clouds at small solar zenith angles forward scattering is the dominate contributor to large IE, but at increased zenith angles outward scattering resembling “reflections” leads to larger IE’s. To facilitate implementation of model results in irradiance modeling, curve fits for the IE profile moving from the edge of the cloud are derived in terms of cloud optical depth and horizontal distance normalized by cloud height.

1. Introduction

Irradiance enhancements (IE) or “over-irradiance” in partly cloudy sky conditions is a well-documented phenomenon defined as a measured irradiance value higher than the expected clear sky maximum (Luoma et al., 2012; Yordanov et al, 2013a,b; Emck and Richter, 2008; Gottschalg et al., 2012; Shade et al., 2007; Pfister et al., 2003). IE is typically ignored in solar resource modeling or forecasting. However, it poses both a threat and opportunity. On the one hand, IE can foreshadow the passage of a cloud and potentially provide information about timing and magnitude of the ensuing down-ramp in power output. On the other hand it can result in temporary elevated power output that steepens the ensuing down-ramp to shaded conditions (Lave et al. 2011), and especially for undersized inverters, can lead to loss of available power through clipping and equipment damage due to high voltages (Luoma et al., 2012). IE absolute magnitudes were hypothesized to be greatest at tropical latitudes in the southern hemisphere, at high elevations

(Yordanev et al., 2013), consistent with the highest recorded event of 1832 W/m^2 at 3400 m above mean sea level (MSL) in the Andes mountains (Emck and Richter, 2008).

IE events were originally thought to be exclusively produced by reflection off the sides of towering cumulus clouds (Segal and Davis, 1992; Pfister et al., 2003; Zehner et al., 2012). Zehner et al. (2012) argued that clouds consisting of mainly water droplets have clear contours, which enable the reflection of photons from their towering sides. Pfister et al (2003) used one year of 1 min averaged data in conjunction with a sky imager to compare the effect of cloud fraction and type on measured enhancement effects, finding that a sky with low cloud fraction of thick cumulus clouds, and with an unobscured solar disk, is most likely to lead to an IE event. This was reasoned to be due to reflections from cloud edges "focusing" diffuse irradiance. However this explanation seems unlikely for a gas-liquid mixture, and is hard to explain with radiative transfer theory, considering the penchant for forward scattering described by Mie theory.

However, more recently there is an increasing body of research suggesting that IE events are mainly due to strong forward scattering of photons inside clouds (Yordanev et al., 2013; Schade et al., 2007). Schade et al (2007) similarly employed a pyranometer and a sky imager in tandem to track IE events; however unlike Pfister et al. (2003) they found that high cloud fraction of thin clouds are more likely to lead to IE events, with the highest IE probability being in near overcast conditions. Yordanev et al. (2013) proposed this is due to the fact that the Mie phase function has a strong peak in the forward direction, with a large portion of all scattered photons concentrated within a scattering angle of 5 degrees. Berg et al. (2011) studied single layer cumulus cloud formations over 8 summers using a total sky imager and pyranometer in tandem with measurement devices of cloud macroscale properties. The authors concluded that IE is most prevalent in spatially and temporally inhomogeneous situations where forward scattered diffuse irradiance (and IE) is significant for small and optically thin clouds.

Despite a large amount of empirical data for IE effects, few have attempted to model the effects with a radiative transfer model (RTM). Segal and Davis (1992) used a Monte Carlo method to model cloud-irradiance interaction. They simulated three different Solar Zenith Angles (SZA) for two different heights (5 km and 10 km) of a two-dimensional (2D) rectangular cloud. The simulations showed IE on the solar side of the cloud edge that extended beyond 10 km horizontal distance in all cases. They also found that as the SZA increased, the magnitude of the IE decreased. However, major drawbacks to their study were (i) a lack of investigation of the spatial surface irradiance profile below the cloud body and (ii) the a-priori assumption that IE is only caused by reflections of the cloud sides. Therefore, the interactions of the photons within or through the cloud body were not investigated.

Bohren and Clothiaux (2006) presented a Monte Carlo RTM to obtain the surface irradiance around a rectangular cloud with changing aspect ratio, but fixed vertical optical depth of 16. A single SZA of zero was used. The authors showed that IE's are noticed around the edges of the cloud, whereas large attenuation was present below the cloud. The magnitude and horizontal extent of the IE was observed to be a function of the cloud aspect ratio. The investigation did not include thinner or thicker clouds and larger SZAs. Zehner et al. (2012) used a three-dimensional (3D) Monte Carlo RTM to investigate the spatial extent and magnitude of IE events around a single cubic cumulus cloud. The same cloud of $\tau = 37.5$ was modeled with increasing cloud base height (100 to 2,000 m) and increasing SZA (20 to 70). The model produced enhancements as large as 40% at the sunfacing edge of the cloud, decreasing in intensity but increasing in area and distance to the cloud shadow with increasing cloud height and increasing SZA. This study also neglects cloud optical depth effects and is neither publicly accessible nor peer reviewed.

Optical depth is expected to have a non-linear effect on IE; very thin clouds do not provide sufficient opportunity for scattering to create IE while in very thick clouds most radiation is attenuated within the cloud, providing an opportunity for IE only further from the cloud edges. Due to the difficulty of measuring optical depth of a cloud accurately, most work has focused on the relative cloud fraction in relation to IE (Schade et al., 2007; Pfister et al., 2003; Tapakis and Charalambides 2014). Pfister et al. (2003) used a trinary cloud classification (clear, thin, and thick) in sky image with measurements to determine that IE's were possible under both thick and thin cloud cover conditions. Both Zehner et al. (2012) and Segal and Davis (1992) looked at the effects of cloud height, but investigated only one optical depth. To the knowledge of the authors, the relationship between optical depth of a cloud and the magnitude of IE it produces has not been investigated to date.

SZA is also expected to influence IE. Tapakis and Charalambides (2013) found that measured IE magnitudes increase monotonically with increasing SZA. The simulation results of Zehner et al. 2012 showed that the area of IE decreases with increasing SZA, but is countered by an increase in peak magnitude. Schade et al. (2007) measurements showed that IE are possible at all SZAs with the greatest likelihood occurring at around 45 degrees for the observed IE. However, these results do normalize out the fact that a SZA of 45 is measured more frequently than SZA angles near the extremes. The results from Segal and Davis (1992) are inconsistent with the measurements of Tapakis and Charalambides (2013) and Schade et al. (2007) as they showed a monotonic decrease in IE magnitude for increasing SZAs. We will examine the influence of IE more holistically to validate these divergent findings and provide conceptual explanations.

Our objective is to classify which optical depths and SZAs are conducive to IE events by simulating the interaction between a cloud and solar irradiance in a 2d Monte Carlo RTM. By varying both the optical depth of a single 2D cloud and the SZA, the variations in the surface irradiance profile can be used to help reconcile the two schools of thought that assign cloud side reflection or within cloud scattering as the primary process that causes IE. Further, functions are fit to the observed IE profiles, such that the insights could be used to improve IE modeling, for example in solar forecasting models. The paper is structured as follows: Section 2 introduces the methods used to investigate the interactions, Section 3 gives the results of this investigation and defines principles which govern IE events, and the final Section concludes the work and provides examples of applications.

2. Radiative Transfer Model

To investigate the causes of IE we use a 2-D Monte Carlo model of SW radiation in the atmosphere, similar to previous studies (Bohren and Clothiaux, 2006; Segal and Davis, 1992). The model consists of a non-absorbing atmosphere with a vertical height of 8 km (one Earth atmospheric scale-height) and a horizontal extent of 50 km. Scattering angle in the atmosphere is estimated via the Rayleigh Phase Function, and a typical total atmospheric optical depth of 0.2 is used (Bodhaine et al., 1999). Since the motivation for this work is harvesting solar energy, the surface is modeled as a perfect absorber. This assumption allows for isolation of the cloud-irradiance interactions without interference from the surface. We assume a characteristic solar wavelength of 530 nm for the photons traveling through our atmosphere since there is little visible wavelength dependency of IE events (Zehner et al., 2010).

A single homogenous water cloud with geometric thickness of 2 km in the horizontal and vertical direction was placed in the center of our model atmosphere (cloud base height (CBH) of 4 km, cloud top height (CTH) of 6km). The 2-D simulation setup effectively means that the simulated cloud is infinitely wide. Ice clouds were not considered in this study since they have been shown to be ineffective at producing IE events (Schade et al., 2007). The width of the atmospheric domain is 25 times greater than that of the cloud in order to investigate IE far from the cloud edge (Segal and Davis, 1992). Similar to the atmosphere, the single scatter albedo (SSA) of the cloud was set to one, since the absorption of photons within the cloud is negligible (Arking, 1996). In order to accurately represent the strong but narrow forward scattering peak observed in liquid water clouds, which is critical to examining the role of forward scattering on IE events (Yordanev et al., 2013), the cloud phase function was estimated to high accuracy by a 1,000 degree Legendre Polynomial. A cloud droplet effective radius (R_{eff}) of 14 μm (King et al., 2013) was used to calculate the phase function, which is typical of cumulus clouds observed at utility scale solar plants in the continental Southwestern US. Vertical cloud optical depth (τ) can then be defined in terms of the cloud liquid water content (*LWC),* R_{eff}, cloud geometric height (h), and liquid water density (ρ_w),

$$\tau = \int_{z=CBH}^{CTH} \frac{3\,LWC}{2\,\rho_w\,r_{eff}}\,dz \tag{1}$$

Thus, the modeled changes in τ are effectively realized via changes in cloud LWC since all other variables are fixed.

In the model simulations we vary τ from 0 (clear sky) to 2 in increments of 0.25 and with a larger non-uniform stepping from $\tau = 3$ to $\tau = 500$. SZA varies from 0° to 60° in steps of 20°. For each unique value of τ and SZA we "fire" 1 billion photons across the 50 km domain (20,000 photons per km), effectively giving the simulation a 0.5 m horizontal resolution. To verify the accuracy of the model it was tested against the SHDOM package (Evans, 1998) under the same scenario. The results were nearly identical. We use the MC method (as opposed to SHDOM) due to its ability to track individual photons, and since it is an exact method limited only by the accuracy of the phase function.

3. Results

3.1 Simple model of irradiance distribution as a function of cloud optical depth

To explain the interaction between irradiance and clouds of different optical depths for the more complex cases that are to follow, a simple simulation was performed. In this simulation, 10,000 photons were fired at SZA = 0°, but only from a fixed location above the center of the cloud for several different optical depths. The results are shown in figure 1, and depicted conceptually in figure 2. For the clear sky case, there exists a large peak at the location where the photons were fired, as expected. With clouds the photons spread over a larger area on the ground, proportional to the optical depth of the cloud. For very thick clouds, the irradiance profile approaches isotropy. As illustrated in Fig. 2, scattering tends to cause the photons of a beam to spread along a forward angle. For only single scattering the distribution of photons by scattering angle is exactly described by the phase function. Multiple scattering, on the other hand, causes the photon distribution to spread further.

In theory, an approximate analytical model could be developed from these results to predict irradiance distribution through a cloud of known τ by superimposing the probability density function (pdf) of Figure 1 over the width of the domain. However, the inset image shows non-linarites near the cloud edge, which would reduce accuracy of such a model. Further, IE at non-zero SZAs may need to be parameterized through effective optical depths or optical paths (τ / cos (SZA)). For these reasons, we elect to use the full Monte Carlo simulation to analyze impacts of SZA and τ, and reserve these results for explanation.

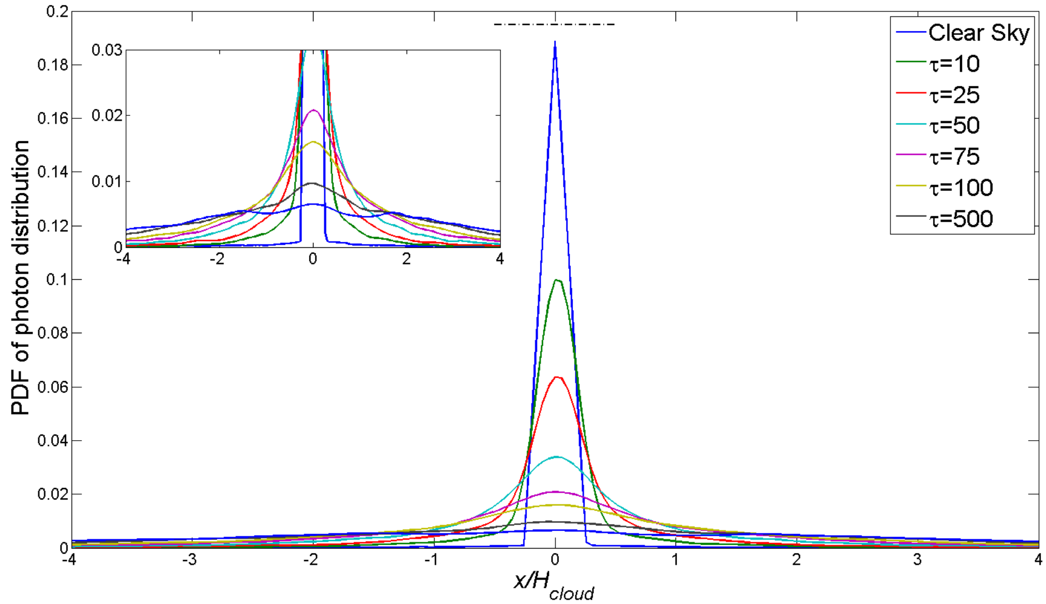

Figure 1:Effect of increasing cloud optical depth on the distribution of photons fired from x/Hcloud=0 across the surface for the sun at zenith. The small inset plot highlights the "spread" of photon distribution with increasing optical depth.

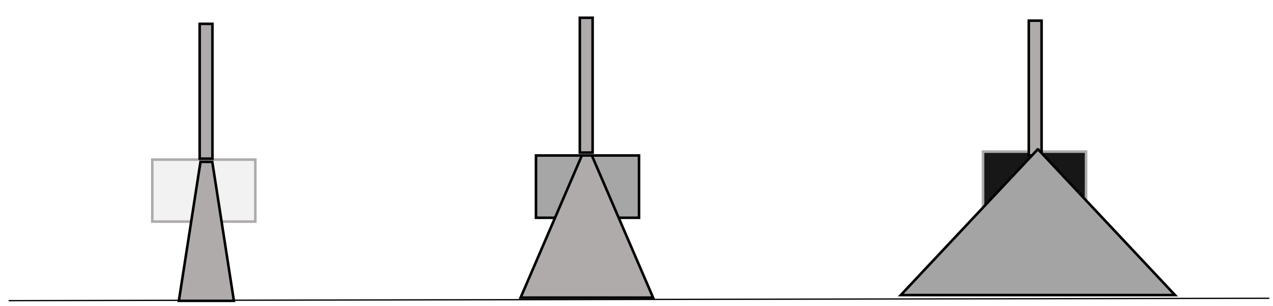

Figure 2: A conceptual depiction of the results of figure 1. In this figure, cloud optical depth increases from left to right, indicated by the darkness of the cloud. Increasing optical depth acts to "spread" the photons over a larger scattering angle.

3.2 Sun at zenith and IE mechanism

For the ensuing simulations, photons are released across the entire length of the domain at the same SZA. Figure 3 shows global horizontal irradiance profiles at the surface, normalized by the clear sky value, for a cloud with eight selected values of optical thickness at a SZA of 0 degrees. At this SZA the magnitude of the IE increases with increasing optical depth up to $\tau = 20$, with a maximum between $20 < \tau < 50$. The IE peaks shortly outward from the cloud edge and then decreases approaching a flat IE profile at about $x/H_{cloud} > 5$ (or 10 km from the edge) depending on the case. Similar to the results of Boren and Clothiaux (2006), except for $\tau = 500$, GHI peaks just beyond the edges of the cloud with a large attenuation directly below the cloud.

The maximum can be attributed to the superposition of unattenuated direct irradiance just outside the cloud edge and diffuse irradiance from photons scattered by the cloud such that they reach the surface just outside the cloud edge. The IE grows with increasing optical depth due to a higher likelihood of scattering. For very thick clouds ($\tau > 50$), the profile flattens in both the IE around the cloud and the attenuation in the cloud shadow. This behavior is consistent with Fig. 1, where the pdfs begin to flatten significantly at $\tau > 50$ indicating a larger spread of photons. The $\tau = 500$ irradiance profile is nearly flat leaving the cloud edge and actually peaks at 1.5 times the cloud height (3 km) away from the cloud edge, with a significantly smaller magnitude than the maximum case. The extreme cloud optical thickness causes a greater proportion of photos to escape the cloud through the edges and at higher altitude. Those photons travel a greater vertical distance than if they exited near the cloud bottom, thus pushing the profile farther from the cloud edge. The total 'enhancement energy' $\left(\int_x^{x\to\infty} \frac{GHI_{surface}}{GHI_{csk}} - 1\, dx\right)$ is also less, due to increased backscatter towards space.

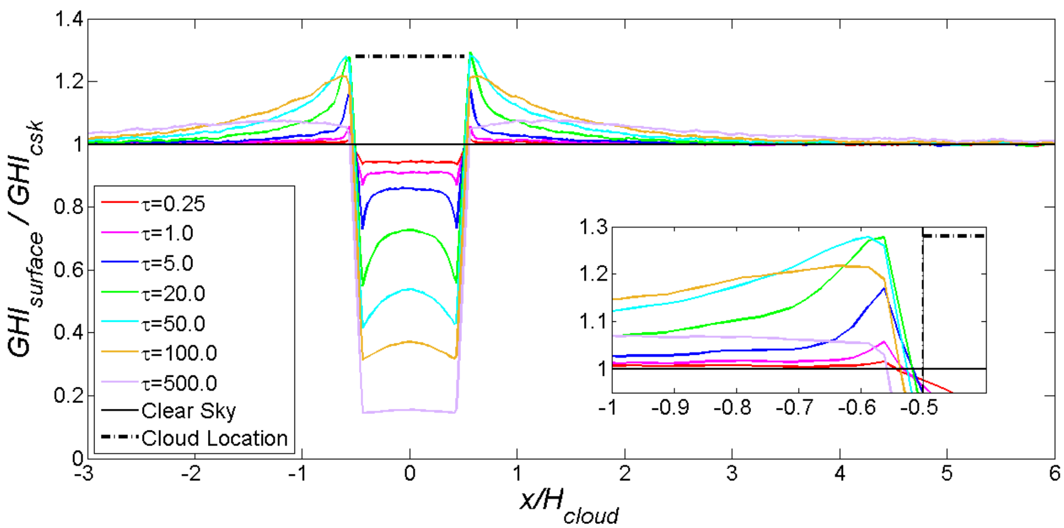

Figure 3: Clear sky normalized global horizontal solar irradiance (clear sky index) profiles at the surface for clouds at eight different optical thicknesses at an overhead zenith. More optical thicknesses were examined, but only selected results are shown for clarity. The cloud extends from -0.5 < x/H_{cloud} < 0.5 (black dashed line). The abscissa is the cloud thickness normalized position. Since the results are symmetric for SZA = 0 the domain is cutoff on the left. The insert provides details just beyond the cloud edge and the vertical black line indicates the position of the cloud edge. Note that all profiles have an enhancement beyond the cloud edge.

While this is not the focus of this paper, the GHI profiles in the cloud shadow also warrant some comments. Given the half-angle of the effective scattering angle distribution from a beam incident on a single column of the cloud (Figs. 1,2), one can distinguish two scenarios for the area shaded by the cloud. If the beam half angle is smaller than the cloud width (here the case for $\tau < 5$), then there exist an area underneath the cloud where the irradiance is horizontally homogeneous; in other words the beam is sufficiently narrow that a point near the center of the cloud shadow does not receive a significant amount of photons from the cloud edges. If on the other hand the beam half angle is larger than the cloud width, then a secondary peak manifests at the cloud center $x / H_{cloud} = 0$, which is a result of the individual scattered beams overlapping most in the center of axisymmetry. In this case any point in the cloud shadow receives a significant amount of photons from all columns of the cloud. The minimum GHI just inward of the cloud edge is the result of the fact that at the cloud shadow edge only beams from one side of the cloud overlap (in other words, the cloud view factor is only ½) and therefore it receives minimal scattered irradiance.

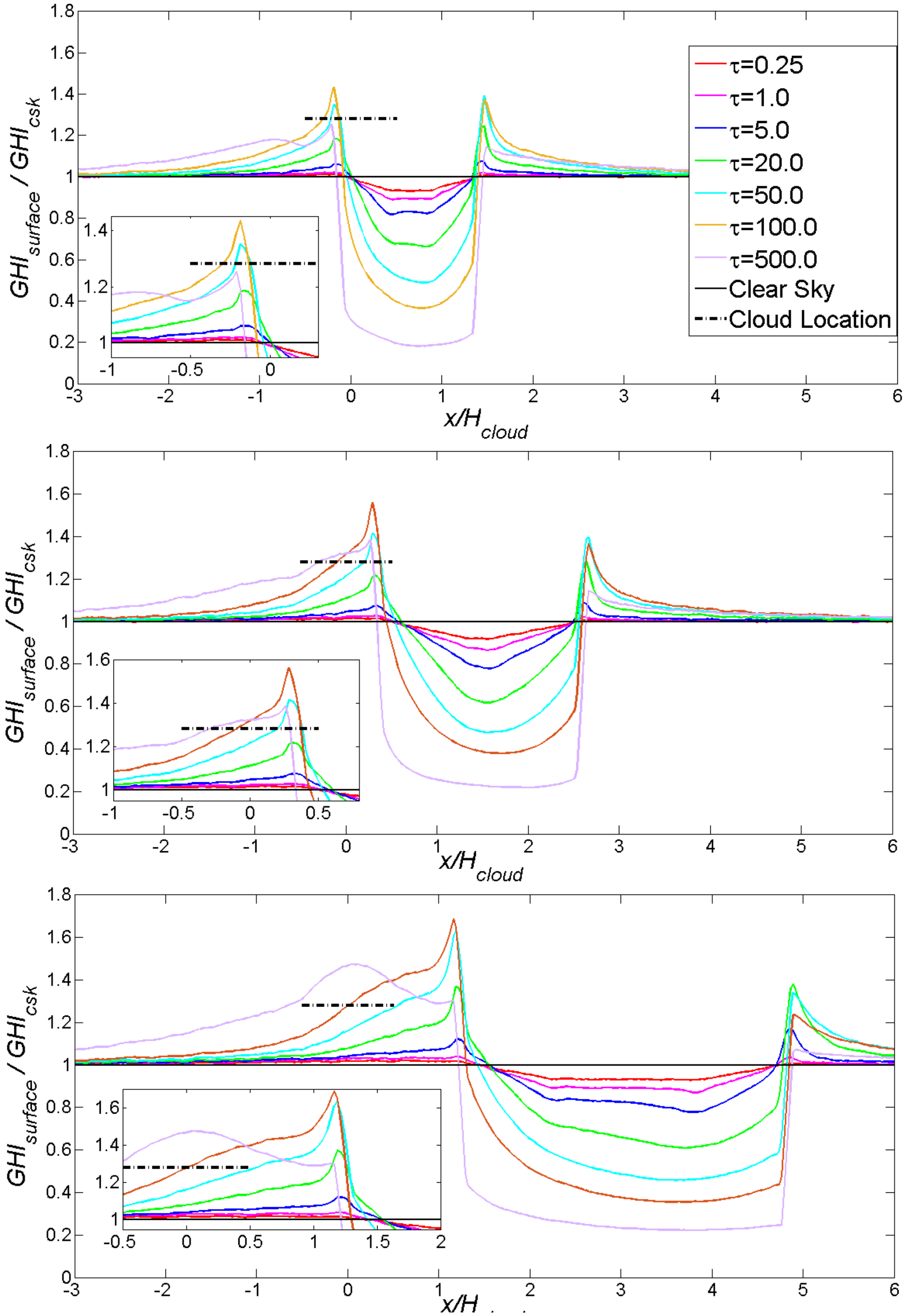

Figure 4: Clear sky index profiles for higher SZA cases for the same eight selected optical depths as given in Fig. 3. a) SZA = 20° b) SZA = 40° c) SZA = 60°.

3.3 Solar zenith angles greater than zero

3.3.1 IE peak magnitude

Figure 4a shows the results for a simulation with SZA of 20°. Increasing the cloud optical depth causes stronger IE, similar to the case with the sun at zenith. However, the symmetry of the peaks is lost and the largest IE is now seen at $50 < \tau < 100$. Similar behavior is observed for larger SZAs of 40º (Fig. 4b) and 60° (Fig. 4c).

For the overhead case the peak IE is 1.3 times the clear sky irradiance value at $\tau = 50$. The greatest IE is found to be 1.7 times the clear sky case, for $\tau = 100$ at SZA = 60º. The peak IE magnitude is consistent with Emck and Richter (2008) and Yordanev et al. (2013a), who measured IEs of approximately 1.5 times the clear sky value. The measured peaks are smaller due to the absorbing atmosphere and since neither group may have observed broken clouds of a thickness as extreme as $\tau = 100$.

3.3.2 IE Peak reversal between sun facing and shaded cloud sides

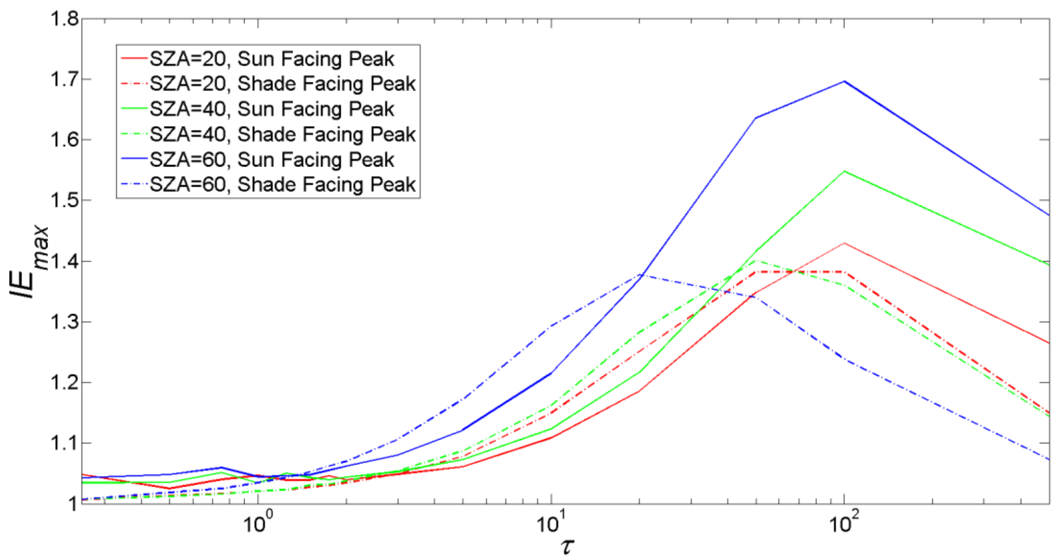

Figure 5: The magnitude of each IE peak plotted against optical depth. The magnitude of both the peak on the sun facing as well as the shade facing side of the surface irradiance profile are shown.

Figure 5 shows the maximum IE of both the sun facing side and the shaded side peak against the cloud optical depth. An interesting feature is that the strongest IE is not always on the sun-facing side. For thin ($\tau \lesssim 1$), clouds, the shaded peak is nearly non-existent, and the sun facing peak has the higher magnitude albeit still small at about 1.05. However, as the optical depth increases ($1 \lesssim \tau \lesssim 20$), the shade facing peak becomes larger than the sun facing peak. For very thick clouds ($\tau \gtrsim 20$), the pattern reverses again such that the sun facing peak is larger. The distinction between thin, moderately thick, and thick clouds depends on the SZA, as observed by the transition of the peak from one side to the other in Fig. 5. Increasing SZA decreases the optical depth at which the peak shifts from the sun facing side to the shaded side (thin to moderately thick), as well as the optical depth at which it shifts back (moderately thick to thick). This is due to the increased effective optical depth (or optical path) at higher SZAs. For this reason the regimes are denoted as approximate in the above description.

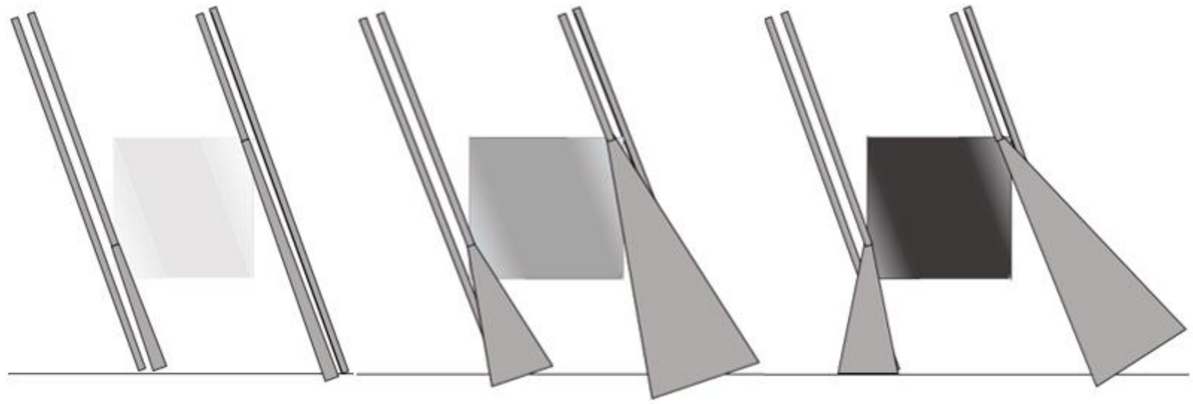

Figure 6: Conceptual depiction of the scattering through effectively thinner cloud corners, leading to different IE peak location. The three scenarios depicted from left to right are for thin, moderately thick, and very thick clouds. Each cloud depicted has a maximum effective optical depth (or optical path) toward the cloud center, with decreasing depth towards the corners, as displayed by the gradient in shading density. Note this depiction is shown for a SZA of 20 degrees, but similar behavior holds for all nonzero SZAs. Note that the cones are plotted to be symmetric about the beam for thin and moderately thick clouds, but are rotated outwards for very thick clouds. This is explained further in the text.

The shift of peak between cloud sides can be explained by referring to Fig. 6, and using the logic developed in Figs. 1-2. Non-zero SZAs have two major effects on the irradiance-cloud interaction. First, the cloud appears as a collection of columns parallel to the SZA with varied effective optical depths or optical paths (τ_{eff}), proportional to the length of the column. For this reason the sun facing bottom and shade facing top corners of the cloud have low τ_{eff} with parallel columns increasing to a higher τ_{eff}, until a constant region of $\tau_{eff_{max}}$ where column length is constant ($|x| < L_{cloud}/2 - \tan(SZA) x H_{cloud}$). Second, the average height of a photon's last scattering event varies, moving upwards with larger cloud optical depth. At a large SZA the photons strike the sun facing bottom corner near the cloud base, and the shade facing top corner near the cloud top. Assuming identical behavior for columns of equal τ_{eff}, photons scattered at a lower height will spread less before reaching the surface, as compared to a larger height.

For very thin clouds, scattering is unlikely and there is a small spread about the forward direction, thus resulting in small peaks on both sides of the cloud, with the sun facing side being slightly more illuminated. For moderately thick clouds, there is a significant amount of scattering events, and the photons are spread further in the forward direction. However, the variation in effective optical depth means the edges have a smaller spread than the center of the cloud (Fig. 1, 2). The spread is even smaller at the sun facing corner, due to its lower altitude, thus contributing less to the IE peak. This trend continues away from the corner, until the regime of constant τ_{eff} is reached. For this reason there is a larger spread of photons on the shade facing side of the cloud, creating a larger IE. For very thick clouds, we expect this trend to continue according to the results in Fig. 1. However, at very large effective optical depths, backscatter dominates, and photons striking the cloud side are more likely to be backscattered / rejected toward the surface than penetrating forward through the cloud. This manifests most strongly for the $\tau = 500$ case in Fig. 4c, where there is so much backscatter that the IE peak moves a significant distance away from the cloud edge.

3.3.3 Shape and location of IE peak

Geometrically, the direct beam is interacting with the cloud between $x_{center} - \text{CBH} \tan(SZA)$ and $x_{center} + \text{CTH} \tan(SZA)$. Since the conceptual model brought forth in Figs. 2 and 6 suggests that IE is strongest near the projected cloud edge, we also expect these locations to coincide with the largest IEs occur. This result is confirmed in Table 1. For the sun-facing side the IE peak occurs slightly outward of the projected cloud edge for SZA = 0 and slightly inward for SZA > 0.

Table 1: Comparison of IE peak location and the projected cloud edge for all SZAs and $\tau = 20$.

	Distance from cloud center (x/H_{cloud})			
	Sun facing peak		Shade facing peak	
SZA	Geometric prediction	Measured Location	Geometric prediction	Measured Location
0	-1	-1.07	1	1.07
20	-0.09	-0.04	2.82	2.96
40	1.52	1.44	5.20	5.24
60	4.20	4.18	9.66	9.79

Edge projection and IE location are not in close proximity for τ = 500 at a SZA of 60 (also SZA 40 to a lesser extent), where IE occurs over a wide region with the peak far away from the projection of the cloud edge; for this particular cloud height the peak IE ends up directly below the cloud (Fig. 4c). As discussed previously, this is due to backscatter out of the sun facing cloud edge.

To isolate the effect of changing SZA on the irradiance profile, the profiles for the highest common IE (τ =50) are plotted together in Fig. 7. In all cases increasing SZA leads to an increase in sun facing edge IE, as well as a loss of symmetry. The result is consistent with the findings of Tapakis and Charalambides (2013), who note that IE magnitudes increase monotonically with increasing SZA. However, as observed in Fig. 5, the shaded IE peak increases monotonically with SZA for thin and moderately thick clouds, but decreases monotonically for thick clouds. This fact may help explain that Schade et al (2009) and Davis and Segal (1992) found contradictory results.

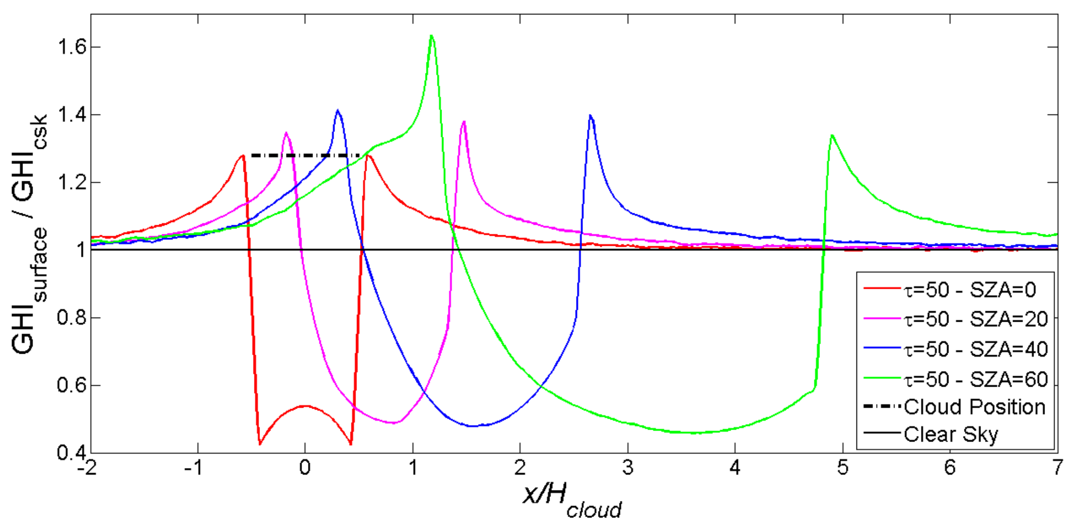

Figure 7: Surface irradiance profile with fixed τ = 50 *for multiple SZA.*

3.4 A simple model for IE

Since it is often not computationally feasible to run a 3D RTM for operational forecasting a simpler analytical solution would be beneficial. Implementing the findings using a first approximation model into a solar forecasting algorithm is possible given *a priori* knowledge of the cloud optical depth, cloud spatial extent, cloud speed, and SZA, all of which can be deduced directly from sky images (Mejia et al. 2015; Ghonima et al. 2012). The IE caused by the most common clouds ($\tau > 50$ is uncommon in broken clouds) can be modeled spatially as an exponentially decaying function away from cloud edges as in Eq. 2

$$IE(X,\tau) = IE_{max}(\tau) * e^{X*C(\tau)}, \tag{2}$$

where $\mathrm{IE_{max}}(\tau)$ is the IE peak, X is the horizontal distance from the projected cloud edge $\left(X = x - \frac{L_{cloud}}{2} . x \geq \frac{L_{cloud}}{2}\right)$, and $\mathrm{C}(\tau)$ is the spatial decay constant associated with the exponential function. Note that each term depends on SZA. Figure 8 provides the relationship of $\mathrm{IE_{max}}(\tau)$ for different SZAs. IE_{max} was found by taking the magnitude of the peak at each of the optical depths listed from Figs. 3 and 4. The function is modeled with a quadratic fit and the fit equation is provide in the figure for SZA = 0.

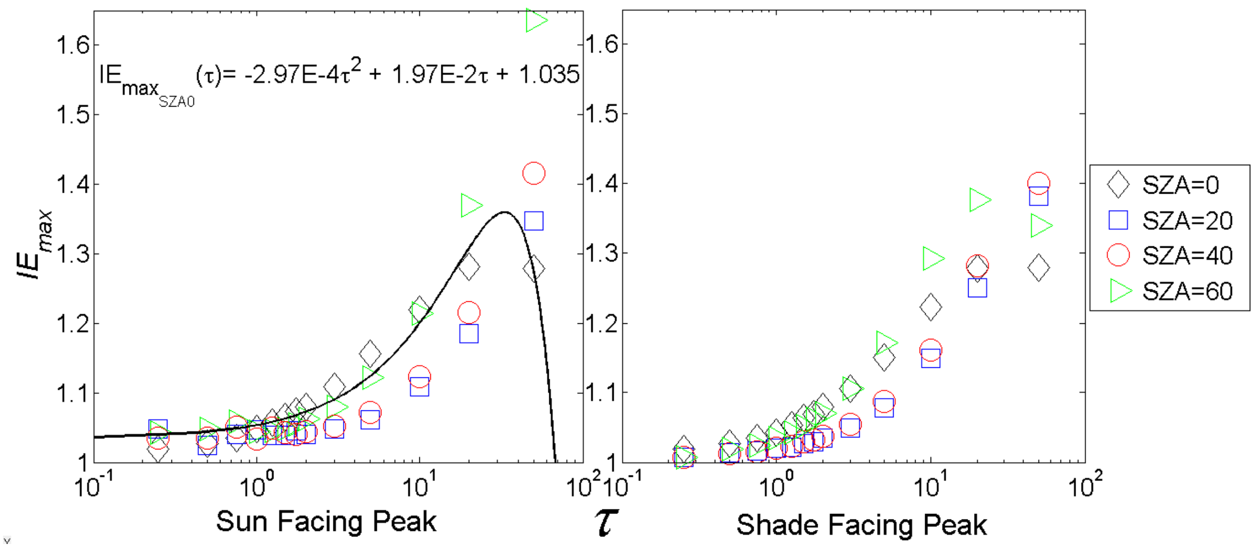

Figure 8: Magnitude of the IE peak versus τ for the four simulated SZAs. The abscissa is limited to τ <50 since these are the clouds most likely to occur in nature. The fit equation for SZA = 0 and the sun facing peak is shown.

Spatially, the IE peak decays exponentially with increasing distance from the cloud edge, at least close to the cloud. Figure 9 is a depiction of the spatial exponential decay coefficients for each optical depth simulated. The trends are consistent with the data presented in Figs. 3 and 4. For the sun at zenith, we see that the peaks are sharp and decay rapidly at small τ, but tend to widen as τ increases leading to a slower rate of decay. For non-zero SZAs we see the opposite trend where low τ causes a wide flat peak, and increasing τ leads to a sharper peak which decays more rapidly. Interestingly we see the results of Fig. 5 manifested in the shade facing peaks. For both SZA = 40° and 60°, for thin clouds ($\tau \lesssim 1$) increasing τ leads to sharper declines. However as we reach moderately thick clouds, the trend reverses due to more forward scattering through the cloud and the peaks begin to widen and decay slowly. The $\mathrm{C}(\tau)$ and $\mathrm{IE_{max}}(\tau)$ relationships can be used together with Eq. 2 to generate a fast empirical model. Table 2 summarizes the equations for $\mathrm{C}(\tau)$ and $\mathrm{IE_{max}}(\tau)$ for all simulated SZA.

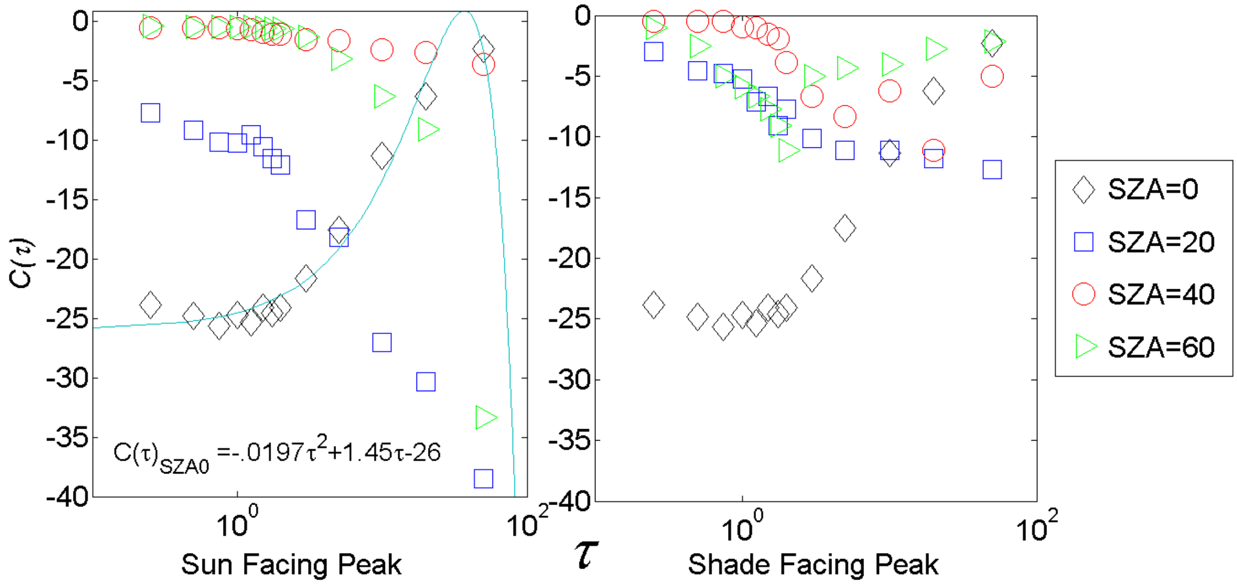

Figure 9: Decay constant C(τ) of Eq. 2 as a function of cloud optical depth. The decay constants are equivalent to the e-folding distance, i.e. the distance from IE_{max}, where the IE is reduced to 1/e of the peak magnitude. The line and equation show the quadratic fit that can be used in Eq. 2.

Table 2: Amplitude and decay constant equations from simulated SZA for all data presented in Figs. 8 and 9 for use with Eq. 2.

	SZA	$IE_{max}(\tau)$	$C(\tau)$
Sun Facing Peak	0^o	$-2.97*10^{-4}\,\tau^2 + 1.97*10^{-2}\,\tau + 1.04$	$-1.97*10^{-2}\,\tau^2 + 1.45\,\tau - 26.0$
	20^o	$-3.80*10^{-5}\,\tau^2 + 8.30*10^{-3}\,\tau + 1.03$	$2.17*10^{-2}\,\tau^2 - 1.67\,\tau - 8.9$
	40^o	$-4.54*10^{-5}\,\tau^2 + 1.00*10^{-3}\,\tau + 1.03$	$2.01*10^{-3}\,\tau^2 - 0.159\,\tau - 0.62$
	60^o	$-1.58*10^{-4}\,\tau^2 + 2.01*10^{-2}\,\tau + 1.03$	$-5.22*10^{-3}\,\tau^2 - 0.401\,\tau - 0.15$
Shade Facing Peak	0^o	$-2.97*10^{-4}\,\tau^2 + 1.97*10^{-2}\,\tau + 1.04$	$-1.97*10^{-2}\,\tau^2 + 1.45\,\tau - 26.0$
	20^o	$-1.64*10^{-4}\,\tau^2 + 1.58*10^{-2} + 1.04$	$8.85*10^{-3}\,\tau^2 - 0.57\tau - 5.86$
	40^o	$-2.00*10^{-4}\,\tau^2 + 1.80*10^{-2}\,\tau + 1.01$	$1.55*10^{-3}\,\tau^2 - 0.85\tau - 0.97$
	60^o	$-4.48*10^{-4}\,\tau^2 + 2.89*10^{2}\,\tau + 1.01$	$-1.75*10^{-3}\,\tau^2 + 0.17\tau - 6.01$

An example of the model is shown in Fig. 10 for $\tau = 10$ and SZA=0. The fit under predicts the IE peak magnitude at this τ, as expected based on Fig. 8, since the quadratic fit underestimates that data point. The model could be improved by using a higher order or different functional fit to the IE_{max} data. The model captures the decay rate accurately within 0.25 x/H from the IE peak. However, beyond that the model decays too rapidly. A double exponential function would better represent the observed dependence, however that is not implemented here since we are primarily interested in the behavior near the peak.

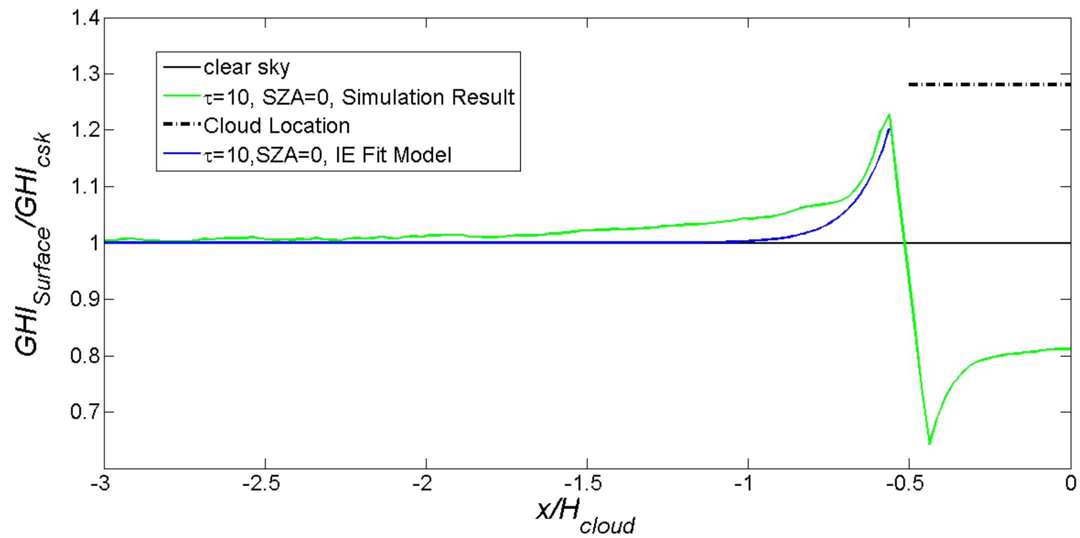

Figure 10: Comparison of the Eq. 2 model to 2D RTM simulation data for $\tau = 10$ and SZA = 0.

4. Conclusions

The surface irradiance profile around a 2D homogenous cloud was simulated by varying its optical depth, as well as the incident SZA using a Monte Carlo radiative transfer model. The model showed that IE occurred due to the presence of the cloud, as expected from empirical evidence. The results along with the explanation show that IE events are due to a superposition of forward Mie scattering of diffuse light with a direct beam at the surface. For extremely thick clouds at large SZAs, multiple scattering lead to rejection of photons from the cloud edge in a manner resembling a "reflection" off the cloud sides.

IE grows in magnitude and spatial extent with increasing τ. This happens due to increased probability of Mie scattering in thick clouds leading to a larger spread of diffuse radiation. Some of the diffuse is scattered outside the projection of the cloud edges, where it is superposed with the direct beam. With the exception of unrealistically thick clouds, peak IE is located less than 0.15 x/H_{cloud} from the geometric projection of the cloud edges. For unrealistically thick clouds, the IE peak moves away from the cloud edge and lessens, but remains elevated for greater distances due to scattering rejection out of the upper cloud sides.

Increasing the SZA leads to an increase in optical path of irradiance, leading to a higher likelihood of both Mie and Rayleigh scattering. This scattering causes a redistribution of photons, which for thin clouds is manifested through a small IE peak on the sun-facing side of the cloud only. For moderately thick clouds, the reduced optical path of the cloud corners causes more photons to be forward scattered through the cloud edges and creates a larger peak on the shaded side of the cloud. However for very thick clouds, the photons striking the cloud face are more likely to be backscattered out towards the surface and the IE peak is again larger on the sun facing side. Differences in IE between sun-facing and shaded side of the clouds are within 10% of clear sky GHI for SZA = 40°, but become large for SZA = 60°.

Our results show that IEs with magnitudes as high 1.63 times the clear sky radiation exist, in agreement with literature where magnitudes as high as 1.5 times the clear sky value have been found in rare cases. It is expected that our magnitude would be lower if atmospheric absorption was considered in the RTM. Yordanev et al. (2013) discuss that the largest IEs may be due to two clouds close to one another with a gap separating them, which acts to magnify the irradiance passing through the gap. Although not shown explicitly, this description is consistent our results and the conceptual model brought forward.

A simple model for the spatial structure of cloud IE was developed. Knowledge of the spatial structure of cloud IE could be implemented into a solar forecasting algorithm if the horizontal extent and optical depth of relevant clouds in the forecast domain was known (Mejia et al. 2015). Combining those metrics along with the cloud speed, it would be possible to predict the magnitude, duration, and position of IE at high resolution. This information could prepare facility and/or grid operators for the up and down ramping associated with the cloud edge passage. In practice, deviations from our results will occur due to different cloud shapes, both in cross section and the 3-dimensionality as opposed to the 2-dimensional clouds considered in our simulations. As described earlier the 3-dimensionality of sun position and cloud position is primarily important at large SZA, while IE is more homogeneous at small SZA. However, since IE will still be caused by Mie scattering processes we project that the conceptual explanations presented here will still apply.

Acknowledgments

We acknowledge Ben Kurtz for his assistance with the design and debugging of the MC RTM used in the study, and Dr. Frank Evans for the insight into RT mechanisms. Funding was provided from the California Solar Initiative RD&D program and a UC San Diego graduate student fellowship.

References

Arking, A. (1996). Absorption of solar energy in the atmosphere: Discrepancy between model and observations. *Science*, *273*(5276), 779.

Berg, L. K., Kassianov, E. I., Long, C. N., & Mills, D. L. (2011). Surface summertime radiative forcing by shallow cumuli at the Atmospheric Radiation Measurement Southern Great Plains site. *Journal of Geophysical Research: Atmospheres (1984–2012)*, *116*(D1).

Bodhaine, B. A., Wood, N. B., Dutton, E. G., & Slusser, J. R. (1999). On Rayleigh optical depth calculations. *Journal of Atmospheric and Oceanic Technology*, *16*(11), 1854-1861.

Bohren, C., & Clothiaux, E. (2006). Fundamentals of atmospheric radiation : An introduction with 400 problems (pp. 323-327). Weinheim: Wiley-VCH.

Emck, P., & Richter, M. (2008). An upper threshold of enhanced global shortwave irradiance in the troposphere derived from field measurements in tropical mountains. *Journal of Applied Meteorology and Climatology*, *47*(11), 2828-2845.

Evans, K. F. (1998). The spherical harmonics discrete ordinate method for three-dimensional atmospheric radiative transfer. *Journal of the Atmospheric Sciences*, *55*(3), 429-446.

Ghonima, M. S., Urquhart, B., Chow, C. W., Shields, J. E., Cazorla, A., & Kleissl, J. (2012). A method for cloud detection and opacity classification based on ground based sky imagery. *Atmospheric Measurement Techniques*, *5*(11), 2881-2892.

Gottschalg, R., Betts, T. R., Mayer, O., Becker, G., Giesler, B., Augel, M., & Weigl, T. (2012). Modelling and validation of spatial irradiance characteristics for localised irradiance fluctuations and enhancements. In *27th European Photovoltaic Solar Energy Conference and Exhibition* (pp. 3801-3804).

King, M. D., Platnick, S., Menzel, W. P., Ackerman, S. A., & Hubanks, P. A. (2013). Spatial and temporal distribution of clouds observed by MODIS onboard the Terra and Aqua satellites. *IEEE Transactions on Geoscience and Remote Sensing*, *51*(7), 3826-3852.

Lave, M., J. Kleissl, Arias-Castro, E., High-frequency fluctuations in clear-sky index, *Solar Energy*, doi:10.1016/j.solener.2011.06.031, 2011

Luoma, J., Kleissl, J., & Murray, K. (2012). Optimal inverter sizing considering cloud enhancement. *Solar Energy*, *86*(1), 421-429.doi:10.1364/BOE.2001069

Mejia, F. A., Kurtz, B., Murray, K., Hinkelman, L. M., Sengupta, M., Xie, Y., and Kleissl, J.: Coupling sky images with three-dimensional radiative transfer models: a new method to estimate cloud optical depth, Atmos. Meas. Tech. Discuss., 8, 11285-11321, doi:10.5194/amtd-8-11285-2015, 2015.

Pfister, G., McKenzie, R. L., Liley, J. B., Thomas, A., Forgan, B. W., & Long, C. N. (2003). Cloud coverage based on all-sky imaging and its impact on surface solar irradiance. *Journal of Applied Meteorology*, *42*(10), 1421-1434.

Segal, M., & Davis, J. (1992). The impact of deep cumulus reflection on the ground-level global irradiance. *Journal of Applied Meteorology*, *31*(2), 217-222.

Schade, N. H., Macke, A., Sandmann, H., & Stick, C. (2007). Enhanced solar global irradiance during cloudy sky conditions. *Meteorologische Zeitschrift*,*16*(3), 295-303.

Tapakis, R., & Charalambides, A. G. (2014). Enhanced values of global irradiance due to the presence of clouds in Eastern Mediterranean. *Renewable Energy*, *62*, 459-467.

Yordanov, G. H., Midtgård, O. M., Saetre, T. O., Nielsen, H. K., & Norum, L. E. (2013). Overirradiance (cloud enhancement) events at high latitudes. *IEEE Journal of Photovoltaics*, *3*(1), 271-277.

Yordanov, G. H., Saetre, T. O., & Midtgard, O. M. (2013). 100-millisecond resolution for accurate overirradiance measurements. *IEEE Journal of Photovoltaics*, *3*(4), 1354-1360.

Zehner, M., Hartmann, M., Weizenbeck, J., Gratzl, T., Weigl, T., Mayer, B., & Mayer, O. (2010). Systematic analysis of meteorological irradiation effects. In *Proc. 25th Eur. Photovolt. Solar Energy Conf. Exhib* (pp. 4545-4548).

Zehner, M., Weigl, T., Hartmann, M., Thaler, S., Schrank, O., Czakalla, M., & Mayer, O. (2011). Energy loss due to irradiance enhancement. In *26th European Solar Energy Conference and exposition, Hamburg*.

Zehner, M., Bung, P., Kathan, V., Schrank, O., Becker, G., Mayer, B., Mayer, O. (n.d.). Modellierung der räumlichen Ausdehnung von Einstrahlungsüber- höhungen und Analyse von deren Abbildung in sehr hoch aufgelösten Datensätzen. 27th PV-Symposium, Bad Staffelstein (Germany, 2012).